Rev.Adv.Mater.Sci. 10 (2005) 387-397

POLYMERIC SUBSTRATES AND ENCAPSULATION FOR FLEXIBLE ELECTRONICS: BONDING STRUCTURE, SURFACE MODIFICATION AND FUNCTIONAL NANOLAYER GROWTH

S. Logothetidis

Aristotle University of Thessaloniki, Physics Department, Lab for Thin Films-Nanosystems and Nanometrology, GR-54124 Thessaloniki, Greece

Received: August 19, 2005

Abstract. In this work, we provide a detailed overview on the incorporation of polymeric substrates, such as Poly(Ethylene Terephthalate)-PET and Poly(Ethylene Naphthalate)-PEN towards the production of future flexible electronics covering all aspects, from surface treatment to the growth mechanisms of transparent functional oxide nanolayers, (e.g. SiO_2) in terms on their bonding structure, surface and interface morphology, stoichiometry, microstructure, optical and mechanical behavior. For this study we have used surface-sensitive, non-destructive characterization techniques, such as in-situ and real-time Spectroscopic Ellipsometry, in an extended spectral region from IR to Vis-farUV, Scanning Probe Microscopies and Nanoindentation in combination to advanced methodologies and modeling procedures.

1. INTRODUCTION

For the last four decades, inorganic silicon and gallium arsenide semiconductors, silicon dioxide insulators, and metals such as copper and aluminum were the backbone of the semiconductor industry. However, nowadays, there has been a radically growing research effort towards the production of Flexible Electronic Devices (FEDs) to take advantage of the semiconducting, conducting, and light emitting properties of organics (polymers, oligomers) and hybrids (organic–inorganic composites) through novel synthesis and self-assembly techniques[1-3]. The use of FEDs, offer substantial rewards by being lightweight, thin, robust, conformable, and have the ability to be rolled when not in use. In addition, plastic-based substrates, coupled with new and intelligent production techniques for the deposition and printing of organic light-emitting polymers and active matrix thin-film transistor arrays, open up the possibility of cost-effective, roll-to-roll processing in high volumes. Thus, they will provide unique technologies and generate new applications to address the growing needs in numerous scientific, technological and industrial areas and in everyday life [1-3].

The performance, efficiency and lifetime of FEDs is greatly affected by the properties of the polymer substrates in which the functional films will be encapsulated. Therefore, the flexible substrate materials should meet specific and advanced demands, in

Corresponding author: S. Logothetidis, e-mail: logot@auth.gr

order to be incorporated in the production of FEDs, such as high optical transparency and high barrier – low permeability in specific gases such as oxygen and water vapour [1-3]. These properties are determined and controlled by the bonding structure of the polymer substrates, the surface nanostructure and chemistry, and also on the functional layers that are developed onto the polymer substrates, and finally on the film-substrate adhesion. Therefore, the detailed knowledge of the bonding structure, mechanical response and surface nanotopography of the polymer substrates are of significant importance and affect all the production steps.

In this work, we provide a detailed overview on the incorporation of polymeric substrates, such as Poly(Ethylene Terephthalate)-PET and Poly(Ethylene Naphthalate)-PEN films towards the production of future flexible electronics. This is an attempt to study all the individual steps of the incorporation of PET and PEN covering from the investigation of their optical properties and the growth mechanisms of the functional oxide nanolayers (e.g. SiO_2, SiO, SiO_x) and their combination to improve the barrier properties of the overall polymer/film system. Also, it is essential to study the surface modification of the polymer films and their functionality for the adherence of the deposited oxide barriers, the mechanical response and the surface nanotopography of the final system to be used for the encapsulation of FEDs.

PET and PEN are excellent candidate materials to be used in the production of FEDs, such as flexible displays and photovoltaic cells by large scale manufacturing processes, since they exhibit a combination of very important properties, as easy processing, good mechanical properties and reasonably high resistance to oxygen and water vapour penetration [4-7]. For the investigation of the optical and mechanical properties of PET and PEN, we have used surface-sensitive, non-destructive characterization techniques, such as in-situ and real-time Spectroscopic Ellipsometry, in an extended spectral region from IR to Vis-fUV, Scanning Probe Microscopies and Nanoindentation in combination to advanced methodologies and modeling and analysis procedures.

2. EXPERIMENTAL DETAILS

The polymer films were industrially supplied PET and PEN samples of thickness of ~12 and ~25 μm, respectively, treated with mechanical biaxial stretching. The SiO_x films were deposited onto the polymer substrates by electron beam evaporation technique in an ultra high vacuum chamber. The surface treatment of the films has been performed at room temperature (RT) by the use of a Pulse DC plasma source using N_2 with gas pressure and flow constant at ~30 mTorr and 40 sccm, respectively whereas the chamber base pressure was P_b=1.2·10^{-7} Torr. Different values of pulsed negative voltage were applied in each of the experiments to the target with a frequency of 100 Hz by a high voltage pulse modulator.

The Spectroscopic Ellipsometry (SE) measurements in the Vis-fUV were performed by a Phase Modulated Spectroscopic Ellipsometer unit from Jobin Yvon/Horiba, in the energy range 1.5-6.5 eV with steps of 20 meV. The SE measurements in the IR spectral range were performed with a Fourier Transform IR Phase Modulated Spectroscopic Ellipsometer. A detailed description of the units has been presented elsewhere [8,9]. The mechanical properties of the films were measured using a NanoIndenter XP system with options for continuous stiffness measurements (CSM) and lateral-force measurements (LFM), placed in a vibration-free isolated cabinet. The hardness (*H*) and elastic modulus (*E*) of each film were measured with a Berkovich, three-sided pyramid diamond indenter, while a special diamond indenter was used for scratch testing. Scratches were made with an edge of the indenter (point-on orientation). An Atomic Force Microscopy (AFM) unit operated in contact and tapping mode and equipped with an Atomic Force Acoustic Microscopy (AFAM) scanner was employed for the investigation and analysis of the surface morphology and nano-topography of the PET and PEN films. The surface topography, as well as the morphological features of both coated and uncoated PET membranes, were measured with Atomic Force Microscope. The instrument functioned in Semi-Contact mode (AC mode), during which the cantilever oscillates above the surface with amplitude approximately in the range of 1-100 nm, and slightly taps the sample once in every oscillation cycle. Cantilevers with nominal spring constant k_c=11.5 N/m and resonance frequency f_o = 230 kHz were used and measurements were taken in ambient and room temperature.

3. RESULTS AND DISCUSSION

In order to replace glass in the production of FEDs, a polymer substrate should have the same structural, optical, mechanical and chemical properties, such as i.e. controllable optical transparency, dimensional, mechanical and thermal stability, chemi-

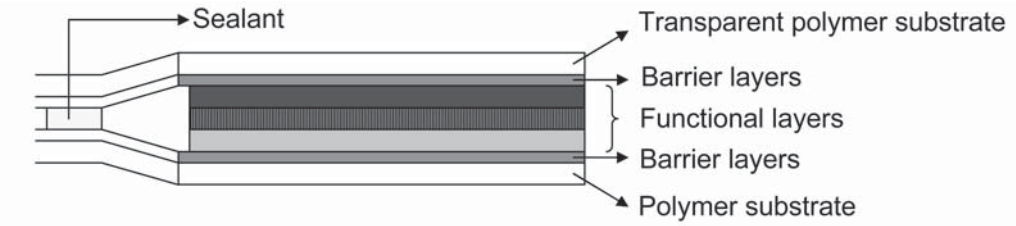

Fig. 1. Structure of a FED, encapsulated in polymer substrates, one of which is transparent, suitable for flexible display devices, e.g. flexible OLEDs.

cal resistance, low coefficient of thermal expansion, smooth surface and finally, enhanced resistance to gas and water vapour penetration. Since no polymer material has all these characteristics, the only way to meet these advanced demands for FEDs encapsulation is to proceed to the production of multilayer composite structure. Such structure is illustrated in Fig. 1.

This structure consists of a base polymer film characterized by good optical transparency, and dimensional stability and smooth surface. The next layer is the barrier film in combination to a hard coating to prevent scratching and to provide solvent resistance. The barrier properties of these layers have to be several orders of magnitude higher than the barrier properties of the uncoated polymer substrate, in order to be used in FEDs with enhanced performance, efficiency and lifetime. Finally, the functional conductive layers are deposited on top, and the whole device is encapsulated by transparent polymer substrate with barrier layer to prevent gas and water vapour penetration to the device. PET and PEN polymer substrates provide an excellent solution to be incorporated in the production of FEDs and the investigation of their adaptation in all process steps, from surface functionalization to the deposition of functional layers.

3.1. Optical properties of PET and PEN polymer films

The unit cell of PET, which is triclinic with a density of 1.455 g/cm^3, is consisted by an aromatic ring and an ester function, that form the terephthalate group, and by a short aliphatic chain that constitutes the ethylene segment [4,5]. PEN exhibits large similarities with PET (has a triclinic unit cell) with the addition of a second phenyl ring, forming the naphthalene group [10]. It can be crystallized into two polymorphs, α and β in both which the ethylene glycol unit has a *trans* conformation, whereas the ester group can adopt the *trans* (α-polymorphism, ρ=1.407 g/cm^3) or the *trans* and *cis* (β-polymorphism, ρ=1.439 g/cm^3) arrangements [9-12]. Although the cell parameters of the PET and PEN monomer units have been extensively investigated by several groups, some representative values are *a*=4.50 Å, *b*=5.90 Å, *c*=10.76 Å, α=100.3°, β=118.6°, γ=110.7°) [4,11,12]. The cell parameters of the two polymorphs of PEN are (a-polymorphism) *a*=6.51Å, *b*=5.75 Å, *c*=13.20 Å, α=81.33°, β=144°, γ=100°, and (β-polymorphism) *a*=9.26 Å, *b*=15.59 Å, *c*=12.73 Å, α=121.6°, β=95.57° and γ=122.52° [4,11,12].

3.1.1. Optical and electronic properties

The optical properties of the PET and PEN films have been investigated by SE from the IR to the Vis-fUV spectral region. SE is based on the determination of the ratio between the parallel and perpendicular complex reflection coefficients, through which the complex dielectric function $\varepsilon(\omega)= \varepsilon_1(\omega) + i\varepsilon_2(\omega)$ is determined. The optical response functions of PET and PEN films in the Vis-fUV spectral region (1.5-6.5 eV) measured with the plane of incidence parallel to the MD, are shown in Fig. 2. The interference fringes that dominate the lower energy region below 4 (PET) and 3 eV (PEN), are Fabry-Perot oscillations due to the multiple reflections of light at the back interface of the polymer films as the result of their optical transparency in this energy region [9,13]. The dielectric function $\varepsilon(\omega)$ of PET at energies above 4 eV, is dominated by four characteristic features, that are arbitrarily assigned to Latin numbers (I, II, III, and IV). A doublet of low intensity absorption bands, are appeared, just above the absorption edge, at around 4.15 (peak I) and 4.3 eV (peak II), whereas two stronger bands are centered at ~ 5.0 (peak III) and 6.3 eV (peak IV). The e(w) of PEN shows similar features due to the similarities in the molecular structure between the monomer units of PET and PEN. However, the ex-

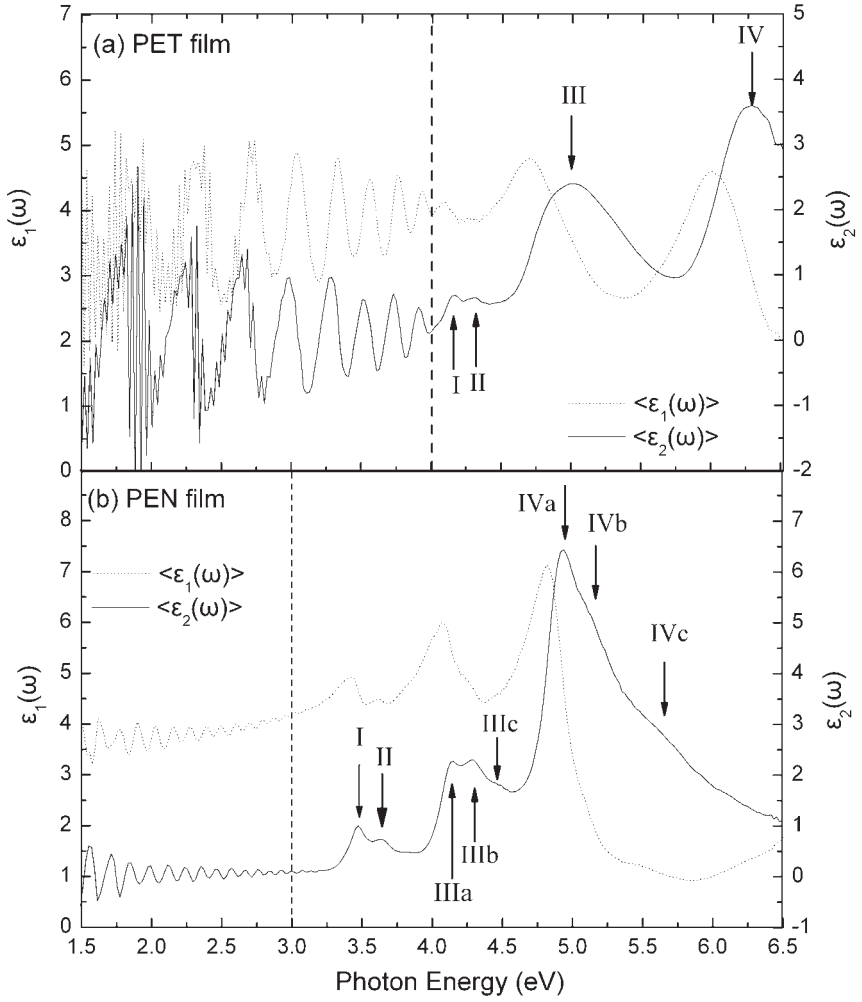

Fig. 2. Dielectric function of PET (a) and PEN (b) films as measured in the Vis-fUV spectral region.

istence of two phenyl rings in the naphthalene group in PEN, instead of the benzene ring in PET, leads to the significant shift of the characteristic absorption bands to lower energies as well as a characteristic split in all of them [14]. Therefore, we observe an energy shift of peaks I and II to 3.4 and 3.6 eV, respectively, although this energy shift is much more pronounced in peaks III and IV, which are appeared at 4.4 and 5.1 eV, respectively, along with a characteristic split in three components.

The peaks I and II have been attributed to the electronic transition of the non-bonded electron of the carbonyl O atom from the n state to the π* unoccupied valence state orbital ($n \rightarrow \pi^*$ transition) [13-16]. The unambiguous assignment of peaks I and II to $n \rightarrow \pi^*$ transition is justified by the study of the polarization dependence of these peaks with the angle between the plane of incidence and the MD, that has been discussed elsewhere [17]. The peak III of PET (PEN), which is possibly attributed to the spin-allowed, orbitally-forbidden $^1A_g \rightarrow {}^1B_u$ transition, is composed by two (three) sub-peaks of parallel polarization dependence [13-16]. The higher broadening can be attributed to the break of the symmetry of the phenyl (naphthalene) rings due to the substitution of carbon atoms. Finally, that peak IV in both PET and PEN has been found to be composed by two sub-peaks with different polarization at 6.33 and 6.44 eV for PET (4.8 and 5.5 eV for PEN) after molecular orbital calculation based on p electron approximation, [13-16] and it can be attributed to the $^1A_g \rightarrow {}^1B_u$ electronic transition of the paradistributed benzene (naphthanene) rings with polarization rules on the plane of the rings [13-16].

The weak intensity and the overlapping of the characteristic peaks corresponding to the electronic transitions of the PET and PEN introduce significant difficulties to the analysis of the $\varepsilon(\omega)$ spectra.

The calculation of the second derivative $d^2\varepsilon(\omega)/d\omega^2$, allows the detailed analysis of the characteristic features that appear much more enhanced than in the undifferentiated spectra. By the analysis of $d^2\varepsilon(\omega)/d\omega^2$, it was found that in PET, the peak II is composed by two weak components; peak IIa at 4.33 and peak IIb at 4.5 eV with the same polarization dependence [14,17]. The very intense peak appeared at ~5 eV (peak III) is composed by two sub-peaks in ~4.9 and ~5.3 eV, characterized by parallel polarization [14,17]. Finally, the peak IV is appeared at ~6.4 eV. Furthermore, in the case of PEN, the peak II is decomposed to peaks IIa and IIb at 3.67 and 3.84 eV, respectively. Also, three components constitute the peak III that are found at 4.15, 4.32, and 4.51 eV assigned as peaks IIIa, IIIb and IIIc, respectively. Finally, the peak IV is decomposed in the three peaks at 4.95, 5.15, and 5.56 eV [14,17].

3.1.2. IR spectral region and vibrational properties

The optical response of PET and PEN films in the IR spectral region are shown in Fig. 3. The strong absorption bands, at 900-1800 cm^{-1}, indicate the contribution of the vibrational modes corresponding to the IR-active chemical bonds of PET and PEN. Above 1800 cm^{-1}, both films are optically transparent and their FTIRSE spectra are dominated by Fabry–Perot oscillations due to the multiple reflections of light at the film interfaces [13]. Among the more intense characteristic vibration bands in the FTIRSE spectra of PET, we observe the vibration modes at ~940 and ~971 cm^{-1} (trans) that could be attributed to the C-O stretching mode, the aromatic CH_2 stretching mode at ~1125 cm^{-1}, the ester mode at ~1255 cm^{-1}, the in-plane deformation of the C-H bond of the para-substituted benzene rings at ~1025 and ~1410 cm^{-1} and furthermore, the characteristic vibration band at 1720 cm^{-1} corresponding to the stretching vibration of the carbonyl C=O groups [18-20]. The band at 1342 cm^{-1} is attributed to the wagging mode of the ethylene glycol CH_2 groups of the *trans* conformations [18-20]. Also, we observe at 1470 cm^{-1} and 1505 cm^{-1} the characteristic peaks corresponding to the CH_2 bending mode, and C-H in plane deformation [18-20].

Due to the existence of naphthalene ring structure in the monomer unit of PEN instead of a benzene ring structure, in PET, the PEN shows a similar IR response, however, with some additional vibration bands. These include the bands at 1098 cm^{-1} that has been attributed to the stretching and

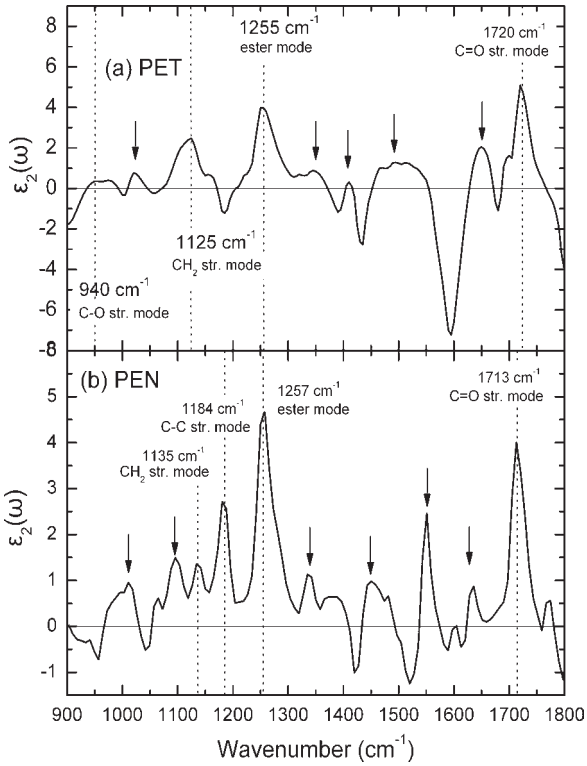

Fig. 3. Imaginary part $\varepsilon_2(\omega)$ of the dielectric function of the PET and PEN films as measured by FTIRSE, where the main vibration bands are shown.

bending modes of ethylene glycol attached to the aromatic structures of the PEN monomer units. Moreover, the characteristic band at 1184 cm^{-1} corresponds to the C-C stretching modes of the naphthalene group. The complex bands at 1335 and 1374 cm^{-1} reveal the bending mode of the ethylene glycol CH_2 group in the *gauche* and *trans* conformations, respectively [14,18-20]. The C=C stretching modes of the aromatic (naphthalene) ring structures of PEN can be observed at ~1635 cm^{-1}. Moreover, the stretching vibration of the carbonyl C=O group appears in lower energy in case of PEN (1713 cm^{-1}) than in PET (1720 cm^{-1}). This could be the result of the increased conjugation due to the existence of naphthalene (PEN) instead of benzene (PET) rings structures, which shifts the maximum absorbance to lower wavenumbers [18-20].

3.2. Surface modification of polymer films

Although PET and PEN polymer films demonstrate a combination of very important characteristics, and especially barrier properties against atmospheric

gases and water vapour, the deposition of subsequent functional thin films onto these polymer substrates represents a prerequisite in order to achieve the necessary and advanced demands for the specific applications. Plasma treatments have been extensively implemented in order to modify many surface properties, such as adhesion, friction, penetrability, wettability, dyeability, and biocompatibility through the induction of physical and chemical surface changes in polymers through several concurrent processes (etching, grafting, polymerization, cross-linking), without modifying their original bulk properties [21,22]. In the framework of this study we have investigated by SE in both IR and Vis-fUV spectral region the modification of the surface properties as induced by N_2 Pulse DC plasma treatment [23].

Fig. 4 shows the changes in the dielectric function $\varepsilon(\omega)$ of PET films in the IR spectral region of 900-1800 cm^{-1}, as induced by the surface modification procedure with N_2 plasma treatment by applying a Pulsed DC voltage of 300, 500, and 700 V. The main absorption bands observed in the FTIRSE spectra of PET seems almost unchanged, due to the small modification depth by the plasma treatment. In order to deduce accurate results from the study of IR spectra after the surface treatment of PET film, we have used the complex optical density *D* defined by the relation $D=\ln(\rho_s/\rho)$, where ρ and ρ_s refer to the complex reflectance ratio $\rho=\tan\Psi e^{i\Delta}$ of the substrate (polymer film) and the surface overlayer modified by the plasma treatment, respectively [24].

By the study of the optical density *D*, it was found that the bond at 1220 cm^{-1} decreases with increasing V_{bias}, while a new vibrational mode is appeared at ~1234 cm^{-1} that could be assigned to C-N or C-O bonds in Φ-NH_2, Φ-NHR, C(=O)-NHR, Φ-OH, Φ-OR or (C=O)-OH is observed after the N_2 plasma treatment. The bond which seems to disappearing at ~1220 cm^{-1} corresponds to the complex ester mode, which is the more susceptible point for etching of the polymer backbone during the plasma treatment. This was justified by the investigation of the ion bombardment dynamics and energy distribution by the Monte Carlo simulation program SRIM (Stopping Ranges Ion in Matter) [25], which revealed that the higher amount of collision energy during the plasma treatment is transported to O_2 atoms on the bombarding material. Also, the oscillator strength corresponding to the stretching vibration of ethylene glycol CH_2 at ~1126 cm^{-1} increases due to the recombination (cross-linking) of the polymer chains after the break of the ester C-O bond resulting to

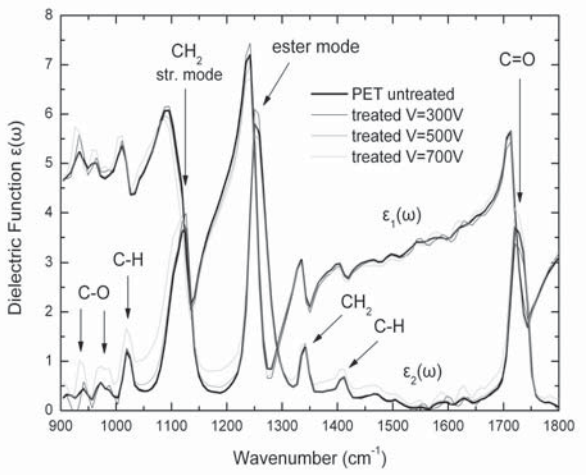

Fig. 4. The real $\varepsilon_1(\omega)$ and imaginary $\varepsilon_2(\omega)$ parts of dielectric function of untreated (◆) PET membrane and after the surface modification with pulsed DC N_2 plasma with voltages of 300, 500 and 700 V [23].

the macromolecular chain scission of the modified overlayer. This is also confirmed by the reduction of the oscillator strength of the vibrational mode of the ester C-O group at ~1250 cm^{-1} denoting the scission of that bond. Moreover, two new vibration bands are also revealed at ~1710 and 1740 cm^{-1} and should correspond respectively to the stretching mode of C=O in C-(C=O)-C or C-(C=O)-O-C bonding structures as a result of the polymer chain cross-linking at the scission point [23].

The effect of the N_2 ion plasma treatment on the electronic structure of the PET films is presented in Fig. 5 where the imaginary part $\varepsilon_2(\omega)$ of the measured $\varepsilon(\omega)$ in the Vis-FUV spectral region, before and after the surface treatment with Pulsed DC N_2 plasma is shown.

For the quantitative determination of the overlayer thickness modified by the N_2 plasma treatment, the Vis-FUV $\varepsilon(\omega)$ were analysed by using a two layer model consisted by the untreated substrate and by a modified PET overlayer described by a) a Lorentz model and b) a Tauc-Lorentz (TL) model [26]. Furthermore, the modified overlayer depth has been estimated also by theoretical calculations by the SRIM program that estimates theoretically the depth of ion penetration into the PET surface, as well as the energy dissipation in the surface range. It was shown that the surface modification is confined in the first surface layers and varies from ~15 nm to 40 nm, depending on the ion energy or the bias voltage applied. However, the calculated thickness

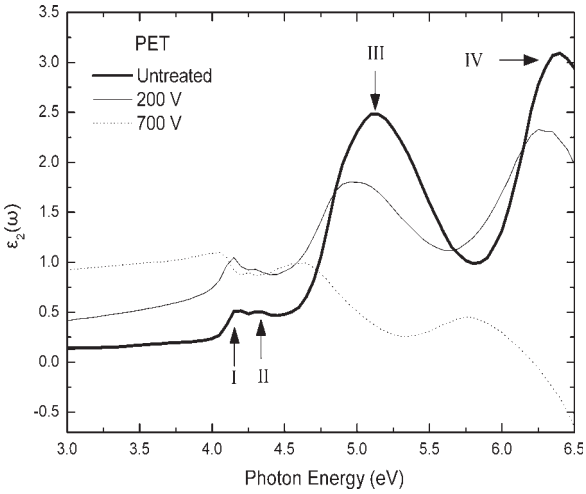

Fig. 5. Imaginary part $\varepsilon_2(\omega)$ of the PET dielectric function before and after surface treatment with pulsed DC N_2 plasma in different bias voltages [23].

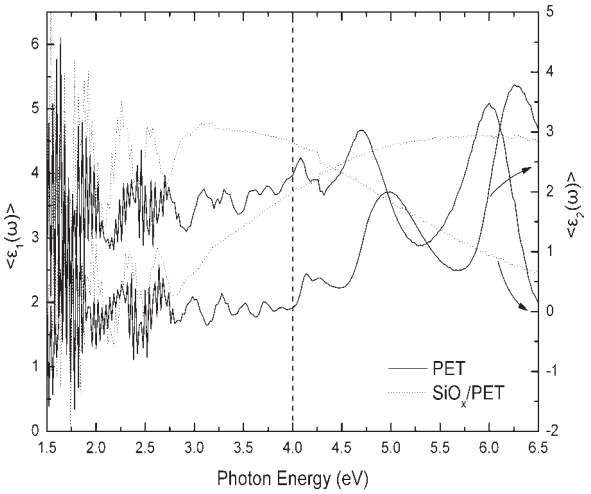

Fig. 6. The real-time evolution of the real and imaginary part of the measured $\varepsilon_2(\omega)$ of a SiO_x film grown on PET film (dotted lines) and the PET film (solid lines) [27].

values by the SRIM simulation have been found to be lower than the values determined by the analysis of the $\varepsilon(\omega)$ spectra, and vary from ~8 to 20 nm for the corresponding ion energies [23]. This is probably due to the fact that SRIM it does not take account of molecular weight of polymer chains of PET film as well as the inhomogeneous nature of surface (oriented and un-oriented regions)[23].

3.3. Deposition of functional layers onto polymer films

The deposition of the SiO_x thin films (x=1 to 2) onto the PET substrate has been investigated in-situ and real-time by Vis-fUV SE. In Fig. 6 the measured pseudodielectric function $\langle\varepsilon(\omega)\rangle$ of the PET substrate, before and after the deposition of the SiO_x system is shown. At the low energy region, the $\langle\varepsilon(\omega)\rangle$ is dominated by interference fringes originated by the multiple reflections of the probing light to the back interface between SiO_x film and the PET substrate. These interference fringes and their lineshape depend strongly on the film thickness and on the stoichiometry of the SiO_x film. That is, when x reaches the value of x=2, the SiO_x film is characterized by higher transparency in comparison to a SiO_x film with x<2 [27]. This fact is evident by comparing the real and imaginary parts of the measured $\langle\varepsilon(\omega)\rangle$ of two representative SiO_x films, having similar thicknesses ~1200 – 1500 Å. The real-time evaluation of the electronic and optical properties of SiO_x films is obtained by fitting using the single Tauc-Lorentz oscillator model, where the imaginary part of the dielectric function is given by [26]:

$$\varepsilon_2(\omega) = \begin{cases} \dfrac{A\omega_0 C(\omega-\omega_g)^2}{(\omega^2-\omega_0^2)^2+C^2\omega^2}\dfrac{1}{\omega} & \omega > \omega_g \\ 0 & \omega \le \omega_g \end{cases} \quad (1)$$

and the real part is $\varepsilon_1(\omega)$ calculated from the Kramers-Kronig integration [26]. The five fitting parameters are: the non-dispersive term ε_∞, the fundamental band gap energy ω_g, the amplitude A, the Lorentz resonant energy ω_0, namely Penn gap, and the broadening term C. The geometrical model assumed for the fitting procedure was the 3-phase model: air/SiO_x film/PET film, and the fitting region was confined within the energy range where the PET film behaves as an absorbing material.

Based on the analysis of the Vis-fUV SE spectra, we derive the time evolution of the SiO_x thickness and its optical properties. The results for the best-fit evolution of thickness d are given in Fig. 7, for the first 50 s of the total deposition time in order to examine in detail the initial stages of growth. These results provide quantitative signatures of the nucleation and growth processes of SiO_2 and SiO materials. The films growth is characterized by the nucleation and coalescence stages that take place at small thicknesses, which is more evident in the case of SiO, and the homogeneous film growth

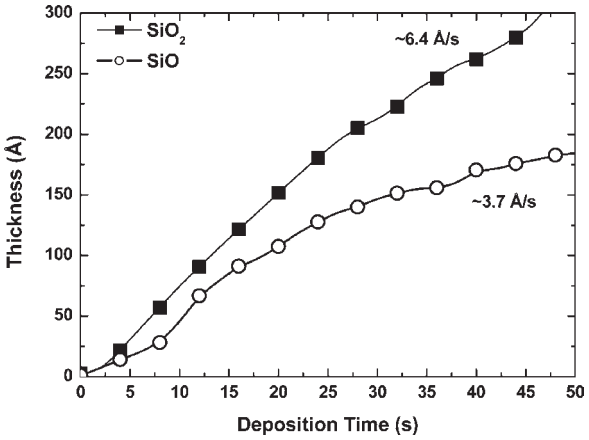

Fig. 7. The evolution of thickness of the SiO_2 and SiO films during the first 50 s of deposition [27].

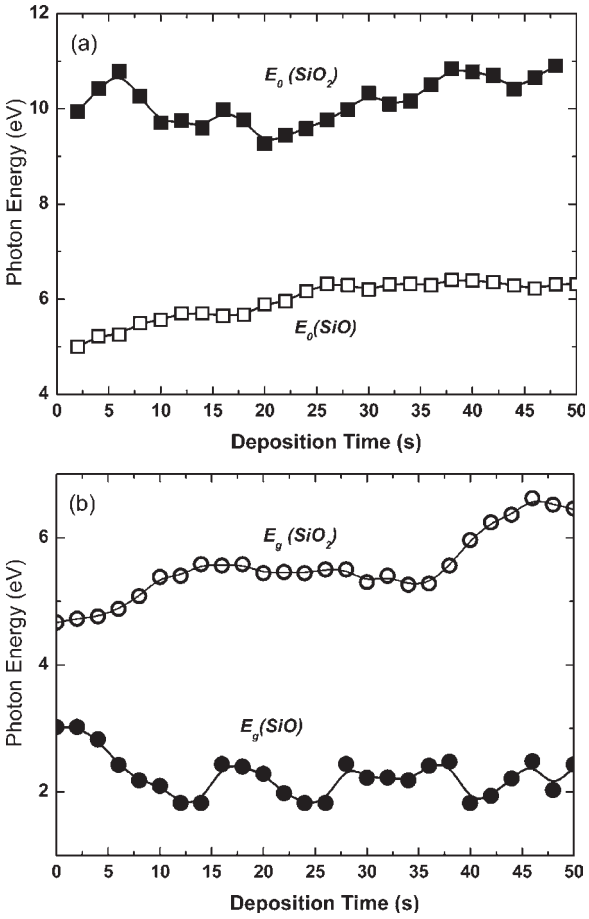

Fig. 8. The evolution of: (a) the E_0 (squares) and (b) E_g (circles) of the SiO_2 and SiO films during the first 50 s of their deposition [27].

stage, through which we can calculate the actual deposition rate; being 6.4 and 3.7 Å/s, for the SiO_2 and SiO, respectively [27]. The differences deduced in the deposition rates between SiO_2 and SiO films are due to the different predominant precursors that can be explained in terms of the used evaporation source material [27].

The electronic and optical properties of the SiO_2 and SiO films can be deduced by the calculated parameters by the $<\varepsilon(\omega)>$ analysis using the TL model. At first, the energy E_0 of the electronic transitions and depends on the stoichiometry of the material. The E_0 shows a significant difference for the SiO_2 and SiO films as it is shown in Fig. 8. In the case of SiO_2 film the E_0 values exhibit fluctuations between 9 and 11eV, and they are eliminated after the completion of the first ~35 s of the deposition time, taking an almost constant value around 11 eV. On the contrary, for the SiO film we obtain a gradual increase in E_0, with its constant value to reach ~6.2 eV. If we take into account the E_0 of the reference SiO_2 and SiO materials, that is 10.8 [28] – 12.0 eV [29] and 5.7 eV [28], respectively, we can verify the respective x values for the studied SiO_2 and SiO films to be in the range $1<x<2$.[27]

The evolution of E_g with the thickness for the two films is also presented in Fig. 8, where it can be seen that the correlation of the E_g values between the SiO_2 and SiO films is similar to that of E_0. The film deposited from SiO_2 evaporation material has the highest E_g compared to the one deposited from SiO evaporation material. This in combination to E_0 means that the excess of the O creates an insulating film, appropriate for microelectronic and optical applications meeting the demands of the optical transparency. The lower percentage of the O in the deposition of the latter film leads to the formation of SiO_x films characterized by stoichiometry close to unity. Therefore, these films can be used as gas and water vapour barriers for packaging applications [27].

3.4. Nanomechanical properties of polymers

The nanomechanical properties of the uncoated PET film and the SiO_x/PET system, with thickness d=60nm and d=145nm, were studied by nanoindentation measurements by employing Continuous Stiffness Measurements (CSM) technique, which gives the advantage of measuring the hardness and the elastic modulus of the samples versus the penetra-

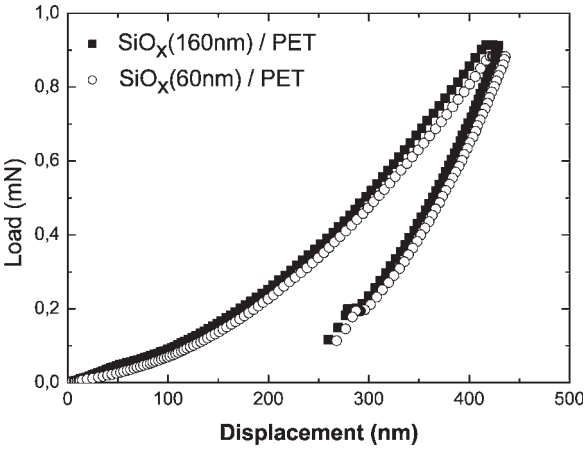

Fig. 9. Loading- unloading indentation curves for the SiO_x coated PET membranes.

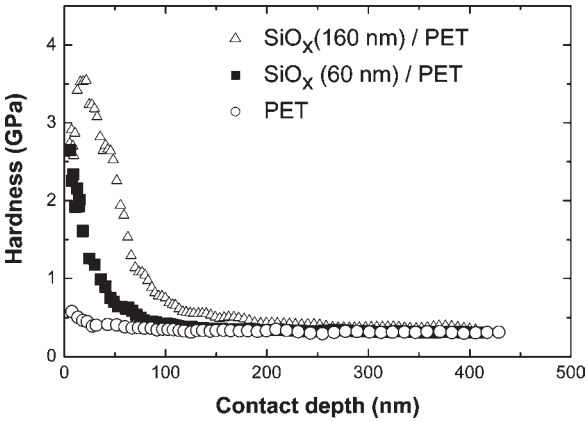

Fig. 10. Hardness evolution versus the contact depth of the SiO_x films deposited onto PET substrate obtained by the CSM technique.

tion depth of the indenter [30]. A Berkovich diamond tip was used as the indenter. The measurements were realized at RT, in acoustically isolated enclosure, and the appropriate corrections were made in order to extract displacements of the indenter due to thermal drift. In Fig. 9 typical loading-unloading curves for the SiO_x thin films (60 and 160 nm) onto the PET substrate vs. the displacement of the indenter are presented. The maximum penetration depth and the applied force were 400 nm and 0.9 mN, respectively, whereas the loading rate was 0.05mN/sec. The absence of any discontinuities in both loading and unloading curves for the two thin films suggests that the SiO_x thin film remains adhere with the substrate, although the indenter's penetration depth exceeds the SiO_x film thickness.

Fig. 10 shows the dependence of the hardness *H* values of the contact depth, measured with the CSM technique, whereas the *H* and *E* values at the samples surface are presented in Table 1. In both coated PET membranes the *H* and *E* values at the surface are significantly higher than those of the uncoated PET, which leads to the conclusion that the deposition of the SiO_x film improved the surface mechanical performance of the PET film. As the indenter penetrates more into the coated PET film the measured values of the *H* and *E* were decreasing and finally coincide with those of the uncoated PET. By comparing the two SiO_x thin films in Table 1, whose thickness is varied, we observe that the thickness increment affect the surface nanomechanical response and in particular both *H* and *E* were found to increase in the case of the thicker SiO_x thin film.

Table 1. Hardness of the SiO_x (60 nm)/PET, SiO_x (160 nm)/PET and PET film obtained by the CSM technique.

Specimen	*H* (GPa)	*E* (GPa)
Uncoated PET	0.48	3.8
SiO_x (60 nm)/PET	2.7	13
SiO_x (160 nm)/PET	3.5	20

3.5. Nanostructural properties

Atomic Force Microscopy (AFM) was employed in order to investigate the nanostructural properties of the SiO_x films deposited onto the PET substrate and their surface morphology. Fig. 11 shows the evolution of the rms surface roughness and the peak-to-peak height as the thickness of the SiO_x layer increases from 60 to 100 nm in relation to the industrial PET substrate. By the study of the AFM images it was revealed that the rms surface roughness and the peak-to-peak height of the 100 nm SiO_x/PET are 0.606 and 5.64 nm, respectively, that those of the industrial PET substrate (0.751 and 6.96 nm, respectively). The above results show that the deposition of the SiO_x layer has a planarizing effect on the PET substrate morphology since dur-

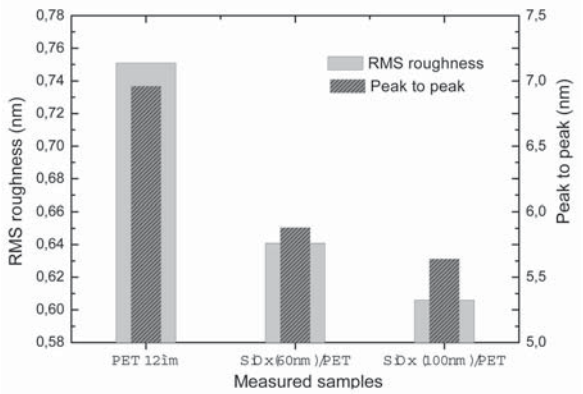

Fig. 11. Dependence of rms roughness and peak-to-peak of the PET samples before and after the deposition of SiO_x coatings.

ing the increase of the SiO_x thickness, the rms surface roughness gradually diminishes.

4. CONCLUSIONS

In this work, we have presented a detailed overview on the investigation of the bonding structure, surface and interface morphology, microstructure, optical and mechanical behavior of PET and PEN polymer substrates. Also, the N_2 plasma surface treatment and the growth of transparent functional oxide nanolayers have been studied. By the study of the optical properties of PET and PEN polymer films in a wide spectral region, the characteristic bands corresponding to the electronic transitions and vibration bands were identified and assigned to the different bonding structures of the PET and PEN monomer units. The N_2 plasma treatment of the PET surface results to the formation of a surface overlayer (with a thickness controlled by the energy of the bombarding N^+ ions), in which the macromolecular chains are characterized by a crosslinked structure. The evolution of the optical properties of the SiO_x/PET system have been investigated by the analysis of the $\varepsilon(\omega)$ measured in situ and real time in the Vis-fUV SE region. By the correlation of the optical properties with the films bonding structure, it was found that the excess of O atoms during the SiO_x growth creates an insulating film, while the lower percentage of O atoms leads to the formation of SiO_x films with *x* close to unity, ideal for gas barriers for packaging applications, as for encapsulation of FEDs. Furthermore, the deposition of the functional oxide layers, leads to the substancial improvement of the surface mechanical performance of the PET polymer substrate, which increases with increasing film thickness. Moreover, the deposition of the functional SiO_x films onto the PET polymer substrate leads to the reduction of the surface roughness of the SiO_x/PET system and the nanotopography of the SiO_x film follow to some extent, the nanotopography of the PET substrate. The above results shortly indicate the potentiality and significance of the use of polymer substrates in combination to inorganic layer systems towards the development of ultra high barrier material combinations fulfilling the future flexible electronic devices application requirements for long-term protection and efficiency.

ACKNOWLEDGEMENTS

This work has been supported partially by the EU GROWTH Project-TransMach (Contract No: G1RD-CT-2000-000334) and the Greek General Secretariat of Research and Technology under PENED-2001 ED 256 Project.

REFERENCES

[1] K. Nomura, H. Ohta, A. Takagi, T.Kamiya, M. Hirano and H. Hosono // *Nature* **432** (2004) 488.
[2] W. Fix, A. Ullmann, J. Ficker and W. Clemens // *Appl. Phys. Lett.* **81** (2002) 9.
[3] M. Losurdo, G. Bruno and E. A. Irene // *J. Appl. Phys.* **94** (2003) 4923.
[4] Y. Wang and S. Lehmann // *Applied Spectroscopy* **53** (1999) 914.
[5] A.E. Tonelli // *Polymer* **43** (2002) 637.
[6] S. R. Forrest // *Nature* **428** (2004) 911.
[7] R. J Hammers // *Nature* **412** (2001) 489.
[8] A. Laskarakis, S. Logothetidis and M. Gioti // *Phys. Rev. B* **64** (2001) 125419.
[9] A. Laskarakis, S. Logothetidis, E. Pavlopoulou and M. Gioti // *Thin Solid Films* **455** (2004) 43.
[10] M. Chtaib *et al.* // *Phys. Rev. B* **44** 19 (1991) 10815.
[11] M. Yanaka *et al.* // *Thin Solid Films* **397** (2001) 176.
[12] Y. Kitano, Y. Kinoshita and T. Ashida // *Polymer* **36** (1995) 10.
[13] A. Laskarakis, M. Gioti, E. Pavlopoulou, N. Poulakis and S. Logothetidis // *Macromol. Symp.* **205** (2004) 95.
[14] A. Laskarakis and S. Logothetidis // *Phys. Rev. B* (2005), in press.
[15] I. Ouchi // *Polymer J.* **15** (1983) 225.

[16] I. Ouchi, I. Nakai and M. Kamada // *Nucl. Instr. Meth. Phys. Res. B* **199** (2003) 270.
[17] A. Laskarakis and S. Logothetidis // *Appl. Phys. Lett.* (2005), submitted.
[18] C. E. Miller and B.E. Eichinger // *Applied Spectroscopy* **44** (1990) 496.
[19] K. C. Cole, J. Guevremont, A.Ajji and M.M.Dumoulin // *Applied Spectroscopy* **48** (1994) 1513.
[20] K. C. Cole, A. Ajji and E. Pellerin, In: *Fourier Transform Spectroscopy*, 11th International Conference, ed. by J. A. de Haseth, (1998).
[21] A. Laskarakis, C. Gravalidis and S. Logothetidis // *Nucl. Instr. Meth. Phys. Res. B* **216** (2004) 131.
[22] T. Tanaka, M. Yoshida, M. Shinohara and T. Takagi // *J. Vac. Sci. Technol. A* **20** (2002) 3.
[23] E. Papaioannou, A. Laskarakis, S. Kassabetis and S. Logothetidis, (2005) submitted.
[24] A. Laskarakis, C. Gravalidis and S. Logothetidis // *Nucl. Instr. and Meth. Phys. Res. B* **216** (2004) 131.
[25] J.F. Ziegler and J.P. Biersack, SRIM-2003 ver. 2003.26, (2003).
[26] G.E. Jelison and F.A. Modine // *Appl. Phys. Lett.* **69** (1996) 371.
[27] S. Logothetidis, 2005, to be published.
[28] *Handbook of Optical Constants of Solids II*, ed. by E.D. Palik (Academic, Boston, 1991).
[29] C.M. Herzinger, B. Johs, W.A. McGaham, J.A. Woollam and W. Paulson // *J. Appl. Phys.* **83** (1998) 3323.
[30] W. C. Oliver and G. M. Pharr // *J. Mater. Res.* **7** (1992) 1564.